Raman self-focusing at maximum coherence

D. R. Walker,* D. D. Yavuz,* M. Y. Shverdin, G. Y. Yin, A. V. Sokolov,† and S. E. Harris

Edward L. Ginzton Laboratory, Stanford University, Stanford, California 94305

Received May 23, 2002

We demonstrate a type of Raman self-focusing and -defocusing that is inherent in operation at maximum coherence. In this regime the two-photon detuning from the Raman resonance controls the refractive index of the medium. © 2002 Optical Society of America

OCIS codes: 020.1670, 190.5650, 190.3270, 320.2250.

It was recently demonstrated[1–3] that a highly coherent Raman medium will generate a collinearly propagating comb of sidebands with many octaves of spectral bandwidth. This is achieved by means of driving a Raman resonance with two single-mode laser fields whose frequency difference is slightly detuned from the Raman resonance and whose intensity is sufficiently large to cause the magnitude of the coherence of this transition to be of the order of its maximum value, $|\rho_{ab}| \approx 0.5$. When this is the case, the generation and the phase-slip lengths become comparable, producing a very broad collinear spectrum. We demonstrated generation of Raman spectra covering the infrared, visible, and ultraviolet regions in molecular D_2 and H_2.[2,3] In related work, Hakuta and co-workers reported the generation of a comb of vibrational sidebands in solid H_2 and rovibrational sidebands in a liquid-hydrogen droplet.[4,5]

The Raman generation process described above significantly affects the propagation of individual sidebands. With reference to Fig. 1, the established molecular coherence ρ_{ab} is, depending on the sign of the Raman detuning $\Delta\omega$, either in phase (phased molecular state) or out of phase (antiphased molecular state) with the strong two-photon drive. Likewise, the refractive indices of the driving lasers are either enhanced for the phased state or reduced for the antiphased state. By operating near maximum molecular coherence, this refractive-index change becomes comparable to the background dispersion, significantly altering the beam propagation and causing either focusing or defocusing of the driving lasers.[6–8]

In this Letter we demonstrate this Raman refractive-index effect. To focus on sideband propagation we drive the Raman resonance with two opposite circularly polarized laser fields and thereby eliminate additional sideband generation.[9] By using the $|\nu'' = 0, J'' = 1\rangle \rightarrow |\nu' = 0, J' = 3\rangle$ rotational transition in low-pressure molecular H_2, we observe focusing or defocusing of the driving lasers. We also give analytical expressions for the refractive indices and demonstrate qualitative agreement between theory and experiment.

There is prior work on self-focusing in stimulated Raman scattering in various media,[10–12] including fibers.[13] There, the excitation is on resonance, and the self-focusing is caused by the nonuniform gain experienced by the propagating beams. There is also extensive literature on Raman-induced Kerr-effect spectroscopy.[14–16] In those works the real and imaginary parts of the third-order Raman susceptibility were probed in the low-coherence regime, and self-focusing and defocusing of the beams were not observed. In other pertinent work, Kawano *et al.*[17] and Losev and Lutsenko[18] demonstrated broad Raman generation with on-resonance excitation. Wittman *et al.*[19] demonstrated efficient Raman generation by impulsive excitation of coherent vibrations and rotations. Bartels *et al.*[20] demonstrated coherent control of vibrational wave packets with shaped short pulses at room temperature.

We describe our system, represented by Fig. 1, with the same formalism used in Ref. 7. Neglecting diffraction and working in local time, $\tau = t - z/c$, we find that the slowly varying envelope propagation equations for the two driving beams (termed the pump and the Stokes) are

$$\frac{\partial E_p}{\partial z} = -j\eta\hbar\omega_p N(a_p\rho_{aa}E_p + d_p\rho_{bb}E_p + b_p^*\rho_{ab}E_s),$$

$$\frac{\partial E_s}{\partial z} = -j\eta\hbar\omega_s N(a_s\rho_{aa}E_s + d_s\rho_{bb}E_s + b_p\rho_{ab}^*E_p), \tag{1}$$

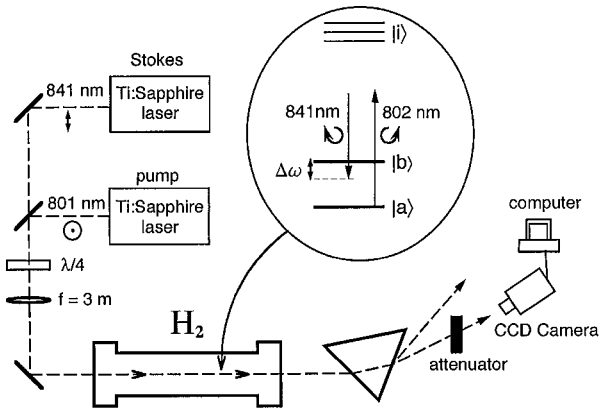

Fig. 1. Experimental setup and energy-level schematic. The applied pump and Stokes lasers with opposite circular polarization coherently drive the Raman transition. As shown, the detuning ($\Delta\omega$) is positive, exciting the phased molecular state.

0146-9592/02/232094-03$15.00/0

where N is the molecule number density and $\eta = (\mu/\epsilon_0)^{1/2}$. The two driving beams are coupled through the molecular coherence ρ_{ab} (off-diagonal density matrix element). Driven off resonance, the molecular medium can be prepared adiabatically, with the sign of ρ_{ab} determined by the sign of the detuning. For $\Delta\omega > 0$, the coherence is in phase with the two-photon drive; for $\Delta\omega < 0$, the coherence is π out of phase with the two-photon drive.[7] For these conditions, we can find the refractive indices of the pump and the Stokes beams by consistently solving Eqs. (1) and the adiabatic solution for the molecular coherence.[7] These refractive indices are

$$n_p(r) = 1 + \frac{N\hbar}{\epsilon_0}\left[a_p\rho_{aa} + d_p\rho_{bb} \pm b_p^*|\rho_{ab}(r)|\frac{|E_s(r)|}{|E_p(r)|}\right],$$

$$n_s(r) = 1 + \frac{N\hbar}{\epsilon_0}\left[a_s\rho_{aa} + d_s\rho_{bb} \pm b_p|\rho_{ab}(r)|\frac{|E_p(r)|}{|E_s(r)|}\right], \tag{2}$$

where r is the transverse radial coordinate (we assume cylindrical symmetry). The sign of the coherence term is positive for the phased state and negative for the antiphased state.

The refractive-index deviation of the Stokes beam [Eqs. (2)] at the center of the transverse profile ($r = 0$) is plotted in Fig. 2(a). The refractive index is enhanced in the phased state and reduced in the antiphased state. Since the refractive index varies over the spatial profile of the beams, self-focusing on the phased side and self-defocusing on the antiphased side occur. Near resonance, the adiabatic approximation fails, and Eqs. (2) no longer hold.

We now proceed with our experimental results, which demonstrate this Raman self-focusing and -defocusing effect. The experimental setup, similar to that reported in Refs. 3 and 9, is shown in Fig. 1. The rotational resonance is driven by two tunable, laboratory-built, Ti:sapphire laser systems at 801 (pump laser) and 841 nm (Stokes laser). Each laser is injection seeded from an external-cavity laser diode and pumped by the second harmonic of a Quanta-Ray Q-switched Nd:YAG laser. The Ti:sapphire lasers produce 60-mJ, 15-ns transform-limited pulses at the seeding laser wavelength. The seeding laser wavelengths can be tuned and are monitored by a Burleigh WA-1500 wavemeter with a resolution of 50 MHz. The laser beams, initially of orthogonal linear polarization, are combined at a dichroic beam splitter and sent through a $\lambda/4$ Fresnel rhomb, changing the beams' polarizations to opposite circular. The laser pulses are focused to a diffraction-limited spot size of $\sim$400 μm in the center of a 50-cm-long H_2 cell, at a pressure of 200 Torr, cooled by liquid N_2 to 77 K.

The beam is analyzed by a commercial beam diagnostic system that consists of a Cohu 6400 Series CCD array camera with a resolution of 24.5 μm $\times$ 19.8 μm, a Beamvision frame grabber, and Analyzer PC software from Coherent. After exiting the cell, the two driving beams are dispersed by an SF14 glass prism. We measure the Stokes beam spatial profile at a distance of 1.5 m from the end of the cell. The beams are captured on the CCD camera, and the beam size is determined by averaging over 50 consecutive shots. The diagnostic software computes the beam size by determining the area of the pixels whose intensity is greater than 50% of the maximum measured pixel value. After exiting the cell, the beams are attenuated with neutral-density filters and two crossed polarizers. The peak intensity seen on the camera is 70% to 95% of the pixel saturation value.

The experimentally obtained beam size of the Stokes beam as a function of the Raman detuning is shown in Fig. 2(b). The beam reaches its maximum and minimum values off resonance, demonstrating the Raman self-focusing and -defocusing effect. For large detunings, molecular coherence becomes negligible, and the beam diameter approaches the value of a freely propagating beam (in the absence of the Raman interaction). We see an abrupt transition from beam maximum to minimum while the tuning goes through resonance.

Figure 3 shows the spatial profile of the Stokes beam for the cases of self-focusing and -defocusing. The pictures are the images from the CCD array. The intensity profile plots show the vertical cross sections

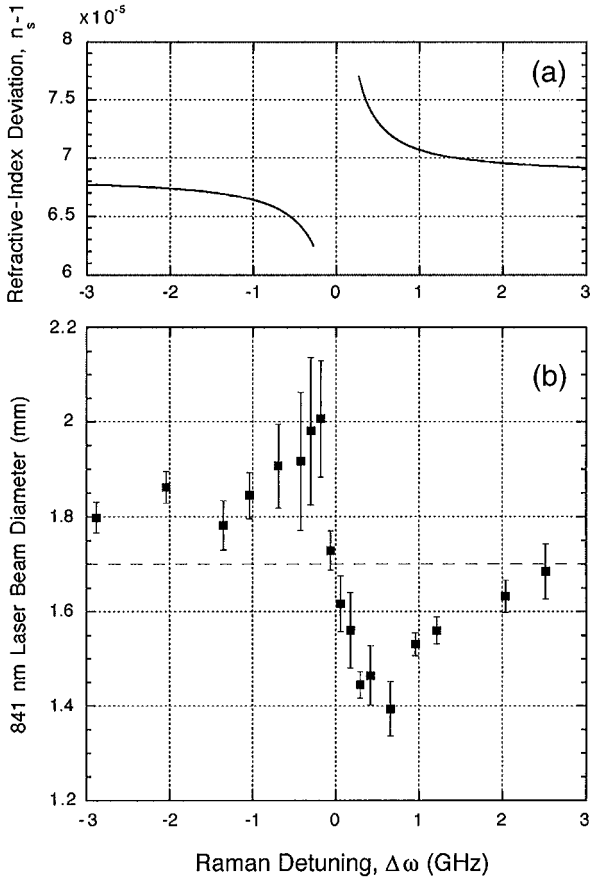

Fig. 2. (a) Refractive index of the Stokes beam above vacuum variation as calculated with Eqs. (2). (b) Stokes beam diameter at FWHM versus the two-photon Raman detuning. Each beam diameter data point is the average of 50 shots; the error bars represent the standard deviation of each data point. The dashed line is the Stokes beam diameter (1.70 $\pm$ 0.03 mm) in the absence of Raman interaction.

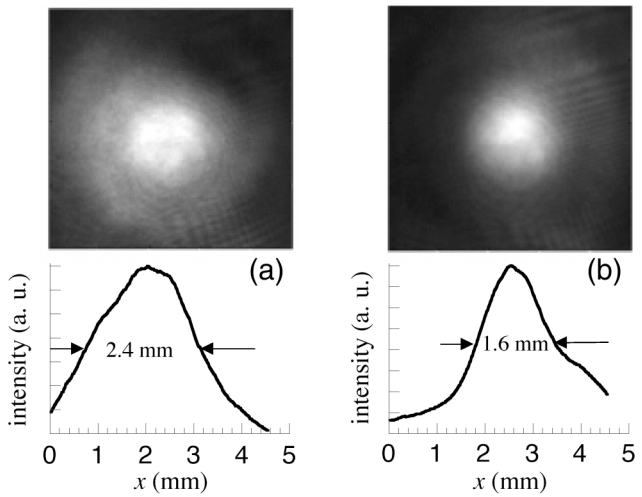

Fig. 3. Stokes beam (a) defocused ($\Delta\omega = -180$ MHz) and (b) focused ($\Delta\omega = 420$ MHz) images captured with a CCD camera. The vertically averaged beam intensity profile is below each image.

averaged over the entire image. Here, when it is defocused, the beam is 50% larger than when it is focused. The approximate Gaussian nature of the beam's intensity is also apparent.

During propagation through the cell, the pump beams do not appreciably change in size. This suggests that the H_2 medium, under the experimental parameters, acts as a thin lens, introducing a curved phase front at the output. The beam then focuses a certain distance from the cell. Assuming low enough coherence ($|\rho_{ab}| < 0.15$) and Gaussian beam propagation, we obtain an analytical formula for the focal length of the Raman medium. The focal length for the Stokes beam is $f_s = \epsilon_0 W_0{}^2 \Delta\omega / 4LN\hbar\eta b_p{}^2 I_p$. Here, L is the Raman cell length, W_0 is the beam diameter before it enters the cell, and I_p is the peak intensity of the pump laser applied to the cell. Calculating the focal length results in $f_s \approx 15$ cm, which is an order of magnitude shorter than our experimental data indicate. We believe that the depletion of the pump and the Stokes beams that is caused by their imperfect polarization and results in some sideband generation is one of the main factors responsible for the discrepancy. After the Fresnel rhomb, we expect several percent of the pump beam's energy to have the same polarization as that of the Stokes beam. Sideband generation, in the same manner as described in Ref. 2, then becomes possible as the process becomes seeded. Because of sideband generation, we see pump and Stokes depletion of up to 30%. Another contributing factor to the observed discrepancy is the imperfect spatial overlap of the two driving beams. In the experiment the beams are slightly asymmetric, and their nonoverlapped parts do not experience the Raman focusing effect.

We have demonstrated Raman self-focusing and -defocusing by coherent excitation of rotational transitions in molecular H_2. Focusing occurs when the molecules are aligned with the laser polarization at the peak of the optical beat note; defocusing occurs when the molecules are antialigned at the envelope peak. Our technique allows the control of the refractive index and, hence, the k vector of propagating lasers in a Raman medium. This may improve beam propagation through turbulent media and allow for phase matching control in processes ranging from four-wave frequency conversion to parametric gain.

The authors thank Scott Sharpe for many helpful discussions. This work was supported by the U.S. Army Research Office, the U.S. Office of Naval Research, and the U.S. Air Force Office of Scientific Research. D. D. Yavuz's e-mail address is dyavuz@stanford.edu.

*These authors have contributed equally to this work.

†Present address, Department of Physics, Texas A&M University, College Station, Texas 77843.

References

1. S. E. Harris and A. V. Sokolov, Phys. Rev. Lett. **81,** 2894 (1998).
2. A. V. Sokolov, D. R. Walker, D. D. Yavuz, G. Y. Yin, and S. E. Harris, Phys. Rev. Lett. **85,** 562 (2000).
3. D. D. Yavuz, D. R. Walker, G. Y. Yin, and S. E. Harris, Opt. Lett. **27,** 769 (2002).
4. J. Q. Liang, M. Katsuragawa, F. Le Kien, and K. Hakuta, Phys. Rev. Lett. **85,** 2474 (2000).
5. S. Uetake, M. Katsuragawa, M. Suzuki, and K. Hakuta, Phys. Rev. A **61,** 011803 (1999).
6. S. E. Harris, Opt. Lett. **19,** 2018 (1994).
7. S. E. Harris and A. V. Sokolov, Phys. Rev. A **55,** R4019 (1997).
8. D. D. Yavuz, A. V. Sokolov, and S. E. Harris, Phys. Rev. Lett. **84,** 75 (2000).
9. A. V. Sokolov, S. J. Sharpe, M. Shverdin, D. R. Walker, D. D. Yavuz, G. Y. Yin, and S. E. Harris, Opt. Lett. **26,** 728 (2001).
10. V. V. Korobkin, A. M. Prokhorov, R. V. Serov, K. F. Shipilov, and T. A. Schmaonov, Phys. Lett. A **47,** 381 (1974).
11. A. D. Kudryavtseva and A. I. Sokolovskaya, Sov. J. Quantum Electron. **4,** 531 (1974).
12. V. A. Isakov, A. P. Kanavin, and I. V. Smetanin, Proc. SPIE **2797,** 18 (1996).
13. G.-S. He, D. Liu, and S.-H. Liu, Opt. Commun. **70,** 145 (1989).
14. G. L. Eesley, M. D. Levenson, and W. M. Tolles, IEEE J. Quantum Electron. **14,** 45 (1978).
15. A. Owyoung, IEEE J. Quantum Electron. **14,** 192 (1978).
16. G. J. Rosasco and W. S. Hurst, Phys. Rev. A **32,** 281 (1985).
17. H. Kawano, Y. Hirakawa, and T. Imasaka, IEEE J. Quantum Electron. **34,** 260 (1998).
18. L. L. Losev and A. P. Lutsenko, Quantum Electron. **23,** 919 (1993).
19. M. Wittman, A. Nazarkin, and G. Korn, Opt. Lett. **26,** 298 (2001).
20. R. A. Bartels, T. C. Weinacht, S. R. Leone, H. C. Kapteyn, and M. M. Murnane, Phys. Rev. Lett. **88,** 033001 (2002).